CVEL

THE CLEMSON UNIVERSITY VEHICULAR ELECTRONICS LABORATORY

TECHNICAL REPORT: CVEL-14-056

Rigorous Derivation of Imbalance Difference Theory for Modeling Radiated Emission Problems

Li Niu and Dr. Todd Hubing

Clemson University

December 20, 2014

This report was submitted for publication. The revised, peer-reviewed version can be found in the following publication:

L. Niu and T. Hubing, "Rigorous Derivation of Imbalance Difference Theory for Modeling Radiated Emission Problems," *IEEE Trans. on Electromagnetic Compatibility*, vol. 57, no. 5, Oct. 2015, pp. 1021-1026.

Table of Contents

Abstract

The imbalance difference theory provides both physical insight and a powerful technique for modeling the conversion from differential-mode signals to common-mode noise, especially for radiated emission problems. Although the theory has been successfully used to model a wide variety of important EMC problems over the past 14 years, it has not been rigorously derived. This paper provides a strict derivation of the theory and carefully defines the important quantities. The derivation demonstrates that imbalance difference calculations are exact provided that the differential-mode propagation is TEM and the current division factor, *h*, represents the actual ratio of currents on the two transmission line conductors excited by a common-mode source. The paper also discusses the acquisition of the current division factor from 2D calculations of the cross-section of the transmission line.

1. Introduction

Unintended radiated emissions can present a challenging EMC problem. These emissions are often caused by unintended common-mode (CM) currents induced on long wires or metal structures[1]-[3]. The generation of CM currents from the known differential-mode (DM) signals has been studied extensively over the last two decades. In [4], for typical printed circuit board (PCB) structures with attached cables, two fundamental common-mode source mechanisms were identified as the current-driven mechanism and voltage-driven mechanism. Current-driven common-mode currents are caused by the signal currents flowing through the partial inductance of the current return path resulting in an effective voltage drop between different portions of the board. Voltage-driven common-mode currents are caused by the electric-field coupling between the signal trace and the attached wires. Although these coupling mechanisms were intuitive, their application required the user to make approximating assumptions, so the results of the calculations were not precise.

More recently, another approach to the problem of modeling differential-mode to common-mode conversion was introduced [5],[6]. This approach is commonly referred to as the Imbalance Difference Theory (IDT). IDT defines the concept of electrical balance in a transmission line (TL) and an imbalance factor (also known as current division factor) that precisely quantifies this balance. IDT demonstrates that changes in the electrical balance on TLs results in a conversion from DM propagation to CM propagation. The amplitude of the induced voltage driving the CM propagation can be accurately expressed as the product of the DM voltage and the change in the imbalance factor at any given point along a transmission line. The IDT provides great insight into the DM-to-CM conversion mechanism and provides an easy way of modeling this conversion in many practical situations. It has been applied to the modeling of many radiated emission problems that would be otherwise difficult to analyze [6]-[19] and has proven to be a very powerful and accurate technique.

Despite its successful application to a wide variety of important EMC problems, IDT has not been widely utilized. Although researchers have shown it to be accurate and reliable, the original papers deriving IDT made simplifying assumptions that seemed to limit the application of the method to structures of little overall interest. The most significant assumption in the original derivation was that both the DM and CM modes exhibited TEM propagation. This appeared to prohibit the application of the theory to radiated emission problems, despite the fact that it seemed to work well for radiated emission modeling.

This paper rigorously derives the IDT for radiated emission problems where no TEM assumption is made for the CM propagation. To avoid confusion, in this paper we will use the term antenna mode (AM), instead of common mode (CM) to describe currents that propagate in one direction on both transmission line conductors without returning on a nearby ground (i.e. the non-TEM case).

2. Definitions of Differential Mode and Antenna Mode Propagation on Transmission Lines

Fig. 1 shows a pair of two-conductor TLs connected end-to-end. The variation in the thicknesses of the bars is to indicate that the left-side TL and the right-side TL have different cross sections. The currents on each conductor, $I_1(z)$ and $I_2(z)$, are generally functions of position. At the interface where the two TLs connect, these currents are continuous with amplitudes I_1 and I_2 as shown in Fig. 1. Throughout this derivation, quantities that are functions of position along the transmission line will be written as functions of z. The value of those quantities at the interface will employ the same variables without being expressed as functions of position.

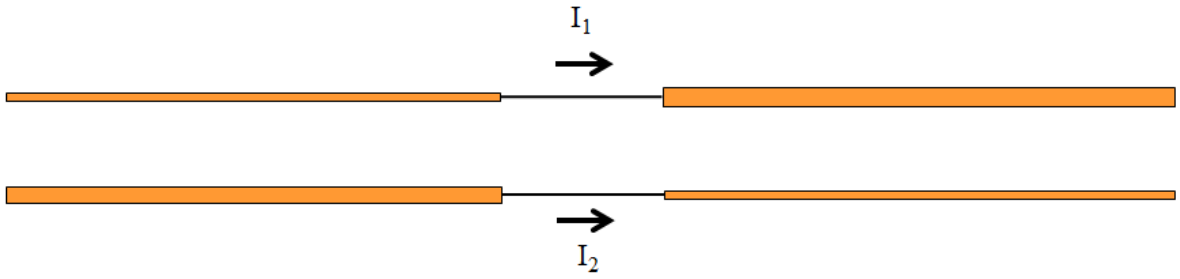

Fig. 1. Two two-conductor TLs with different cross sections connected end-to-end.

2.1 Definition of Antenna Mode Signals

The antenna-mode current, I_{AM} is defined as the total current that flows on both conductors,

$$I_{AM}(z) = I_1(z) + I_2(z)\,. \tag{1}$$

The antenna-mode impedance at the interface, Z_{AM}, is defined as the input impedance of the antenna that is formed by the conductors in Fig. 1 and when it is driven by a source as indicated in Fig. 2.

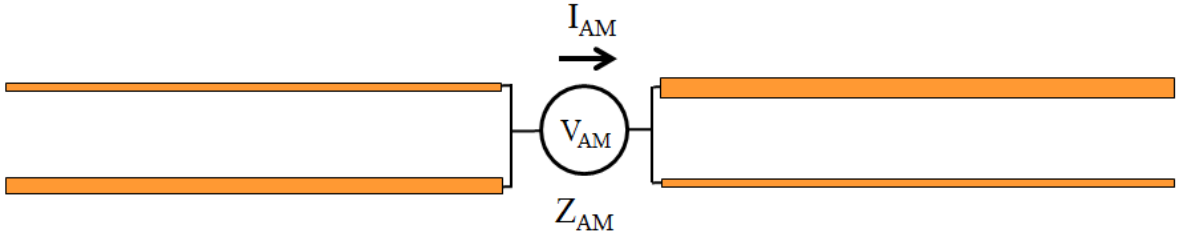

Fig. 2. The antenna-mode voltage at the interface between the TLs.

The AM voltage, V_{AM}, is defined as the product of the AM current and the AM impedance at the interface,

$$V_{AM} = I_{AM} \cdot Z_{AM}\,. \tag{2}$$

2.2 Definition of Current Division Factor

The AM current is carried by both conductors of the TLs. We define the current division factor, h, as the portion of the AM current that flows on one conductor divided by the total AM current flowing on both conductors.

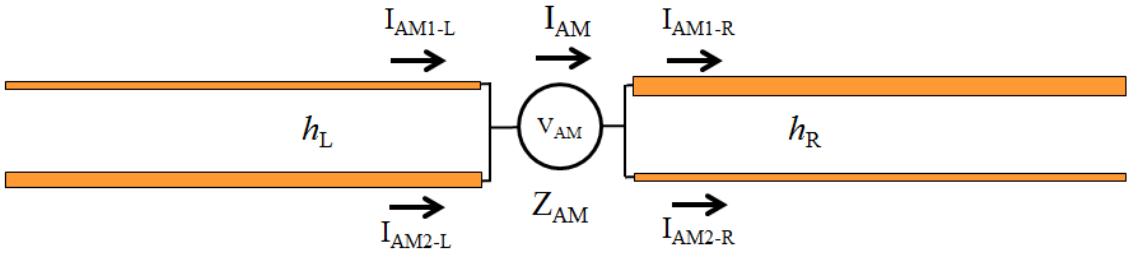

Fig. 3. Antenna mode of TLs with divided AM currents.

In Fig. 3, $I_{AM\text{-}1L}$, $I_{AM\text{-}2L}$, $I_{AM\text{-}1R}$ and $I_{AM\text{-}1R}$ denote the current on each conductor of the TLs at the points just to the left and right of the interface, respectively. Due to the continuity of the currents I_1 and I_2, they satisfy the following relationship:

$$I_{AM} = I_{AM1-L} + I_{AM2-L} = I_{AM1-R} + I_{AM2-R} \ . \tag{3}$$

At the interface, we denote the current division factors for the left-side and right-side of the TL as h_L and h_R. These factors are defined as,

$$h_L = I_{AM1-L} / I_{AM} \ , \tag{4}$$

$$h_R = I_{AM1-R} / I_{AM} \ . \tag{5}$$

Combining (3), (4) and (5), the AM current on each conductor can be expressed as:

$$I_{AM1-L} = I_{AM} \cdot h_L \ , \tag{6}$$

$$I_{AM2-L} = I_{AM} \cdot (1-h_L) \ , \tag{7}$$

$$I_{AM1-R} = I_{AM} \cdot h_R \ , \tag{8}$$

$$I_{AM2-R} = I_{AM} \cdot (1-h_R) \ . \tag{9}$$

2.3 Definition of Differential Mode Signals

The DM signals on the TLs are TEM, so we can define the DM voltage, $V_{DM}(z)$, as the voltage difference between the two conductors. V_{DM} specifically represents the DM voltage at the interface, as shown in Fig. 4.

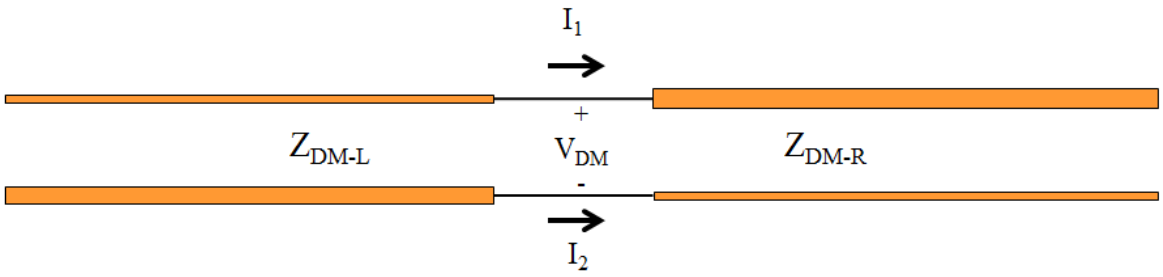

Fig. 4. Differential-mode voltage at the interface of two two-conductor TLs.

The DM impedance, Z_{DM}, is defined as the characteristic impedance of the TLs. They are denoted as $Z_{DM\text{-}L}$ and $Z_{DM\text{-}R}$ for the left-side and right-side of the TLs.

The AM current was defined in (1). We want the differential mode and the antenna mode to be orthogonal, so we define the DM current to be the current remaining when the AM current is subtracted from the total current. This means, that the DM components of current have the same amplitude and

opposite direction on each conductor. The DM components of the current on each side of the interface can be expressed as,

$$I_{DM-L} = I_1 - I_{AM1-L} = -(I_2 - I_{AM2-L}) = (1-h_L)\cdot I_1 - h_L \cdot I_2 \text{ ,} \quad (10)$$

$$I_{DM-R} = I_1 - I_{AM1-R} = -(I_2 - I_{AM2-R}) = (1-h_R)\cdot I_1 - h_R \cdot I_2 \text{ .} \quad (11)$$

3. Conversion between DM signals and AM signals on TLs

The AM circuit in Fig. 3 can be represented equivalently as shown in Fig. 5. In this figure, the voltages between the 4 conductors at the interface are identical to their values in Fig. 3.

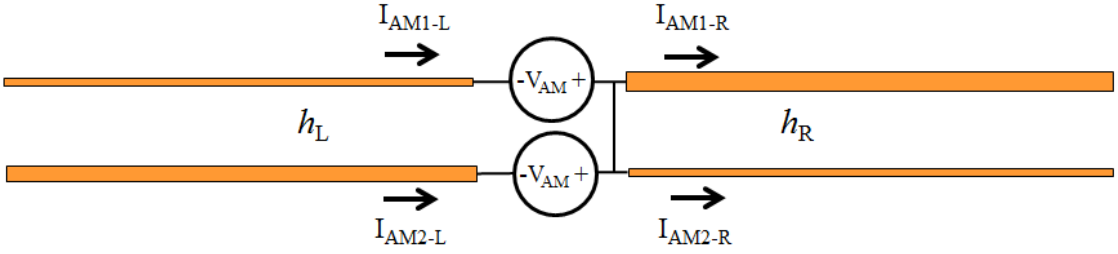

Fig. 5. Equivalent AM circuit.

Applying superposition, the AM circuit of Fig. 5 can be decomposed into the two circuits in Fig. 6 and Fig. 7.

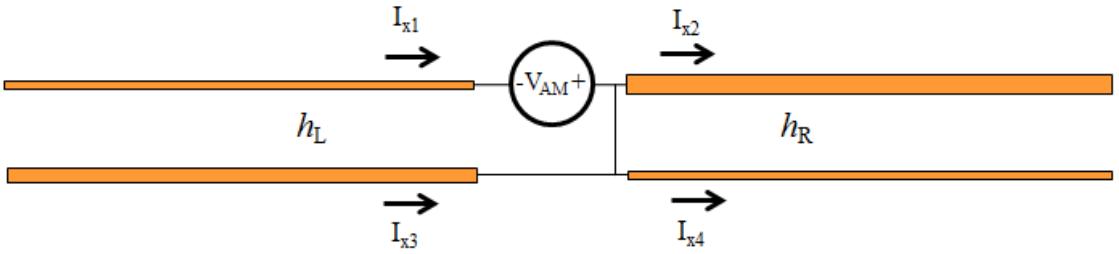

Fig. 6. Decomposition of AM circuit (1/2).

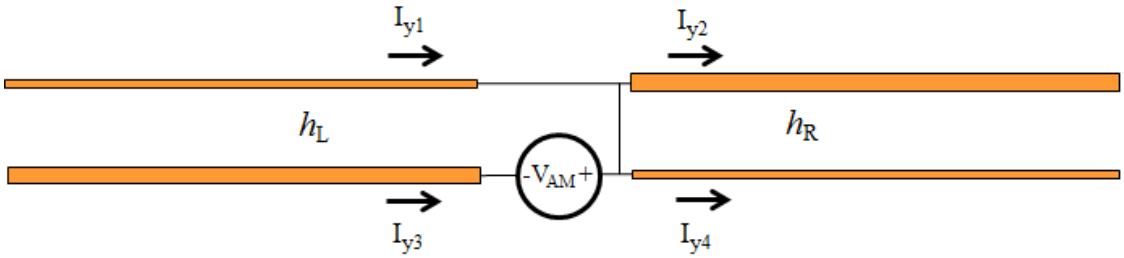

Fig. 7. Decomposition of AM circuit (2/2).

The current on each conductor in Fig. 5 can be expressed as the sum of the corresponding currents on the same conductor in Fig. 6 and Fig. 7 (denoted as "I_x"s and "I_y"s):

$$I_{AM1-L} = I_{x1} + I_{y1} \text{ ,} \quad (12)$$

$$I_{AM1-R} = I_{x2} + I_{y2} \text{ ,} \quad (13)$$

$$I_{AM2-L} = I_{x3} + I_{y3}\,, \tag{14}$$

$$I_{AM2-R} = I_{x4} + I_{y4}\ . \tag{15}$$

The continuity of the current ensures that,

$$I_{x1} + I_{x3} = I_{x2} + I_{x4}\ , \tag{16}$$

$$I_{y1} + I_{y3} = I_{y2} + I_{y4}\ . \tag{17}$$

In Fig. 6 and Fig. 7, the ideal voltage source V_{AM} drives three conductors relative to the fourth one. The configurations in Fig. 6 and Fig. 7 can be redrawn equivalently as shown in Fig. 8 and Fig. 9, respectively.

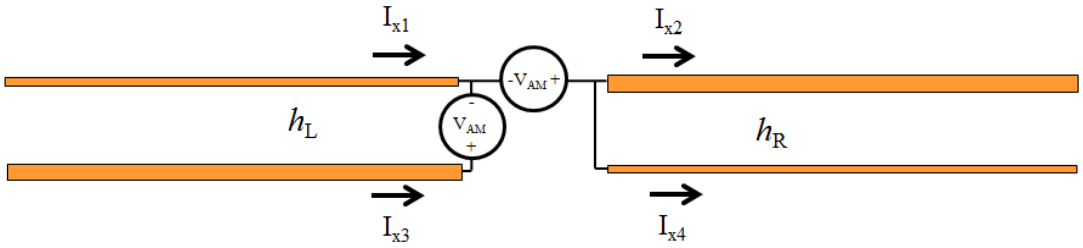

Fig. 8. Equivalent to AM circuit (1/2) in Fig. 6.

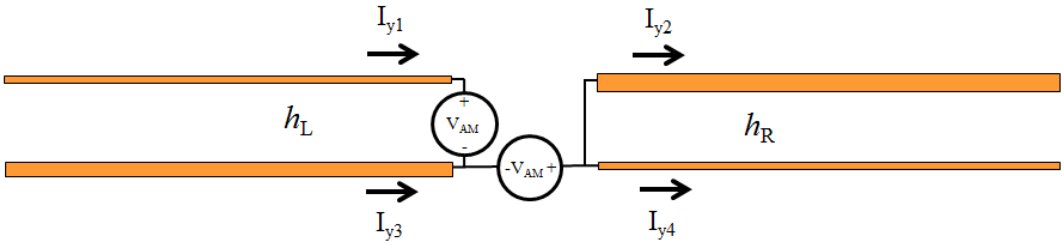

Fig. 9. Equivalent to AM circuit (2/2) in Fig. 7.

Examination of these circuits reveals that the current on the lower left conductor, I_{x3}, in Fig. 8, and the current on the upper left conductor, I_{y1}, in Fig. 9, are due to the same source voltage, V_{AM}, driving the same load impedance, the DM impedance of the left-side TL. As a result these currents are equal,

$$I_{x3} = I_{y1}\ . \tag{18}$$

Substituting I_{y1} in (12) with I_{x3} and combining the result with (16), we get,

$$I_{AM1-L} = I_{x1} + I_{x3} = I_{x2} + I_{x4}\ . \tag{19}$$

It is interesting to note that the total AM current on the circuit in Fig. 8 is equal to the portion of the AM current that flows on the upper conductor on the left-side TL in Fig. 3. Similarly, the total AM current in the circuit of Fig. 9 is equal to the portion of AM current that flows on the lower conductor of the left-side TL in Fig. 3.

Using a similar approach, we can represent the original AM circuit of Fig. 3 as shown in Fig. 10. This circuit can be decomposed into the two circuits shown in Figs. 11 and 12.

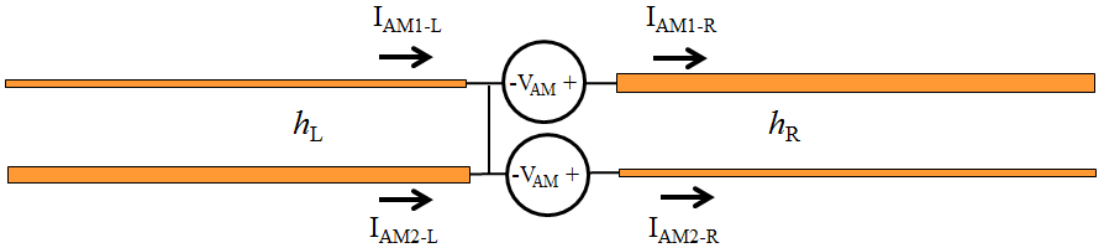

Fig. 10. Equivalent AM circuit.

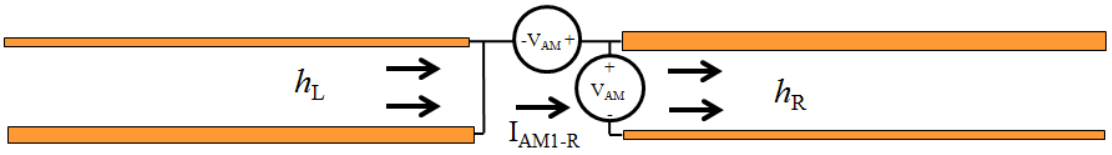

Fig. 11. Decomposition of AM circuit (1/2).

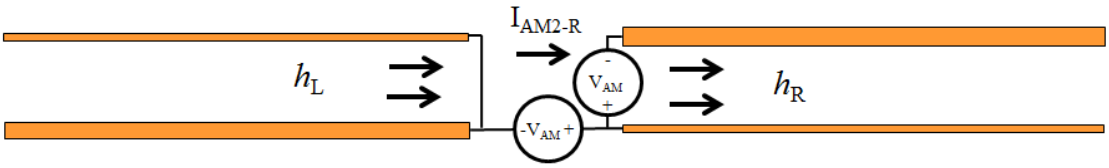

Fig. 12. Decomposition of AM circuit (2/2).

We can define partial AM impedances as follows,

$$\begin{aligned} Z_{AM1L} &\equiv Z_{AM} / h_L, \\ Z_{AM2L} &\equiv Z_{AM} / (1-h_L), \\ Z_{AM1R} &\equiv Z_{AM} / h_R, \\ Z_{AM2R} &\equiv Z_{AM} / (1-h_R). \end{aligned} \tag{20}$$

The partial AM impedances are the impedances seen by the voltage sources in Fig. 8, Fig. 9, Fig. 11, and Fig. 12. The AM currents associated with these circuits are:

$$\begin{aligned} I_{AM1-L} &= V_{AM} / Z_{AM1-L}, \\ I_{AM2-L} &= V_{AM} / Z_{AM2-L}, \\ I_{AM1-R} &= V_{AM} / Z_{AM1-R}, \\ I_{AM2-R} &= V_{AM} / Z_{AM2-R}. \end{aligned} \tag{21}$$

Referring back to the original circuit in Fig. 1, the DM voltage at the interface is V_{DM}. Placing two ideal voltage sources with amplitude of V_{DM} in parallel at the interface, as indicated in Fig. 13, does not change these currents.

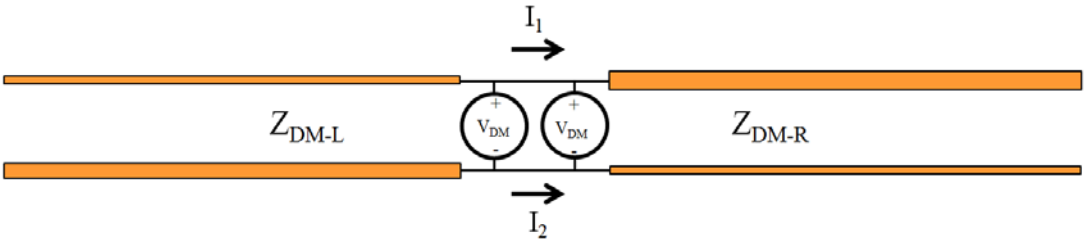

Fig. 13. A circuit equivalent to the original circuit in Fig. 1.

Placing two additional ideal voltage sources in series with the same amplitude, V_{DM}, and opposite sign, as shown in Fig. 14, does not change these currents either.

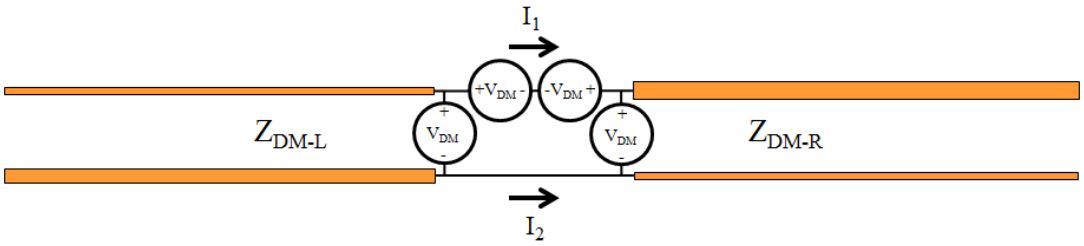

Fig. 14. Another circuit equivalent to the original circuit in Fig. 1.

Using superposition, the circuit in Fig. 14 can be decomposed into the two circuits shown in Fig. 15 and Fig. 16.

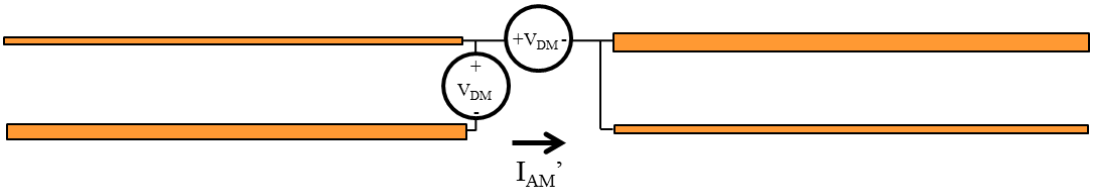

Fig. 15. Decomposition of the original circuit (1/2).

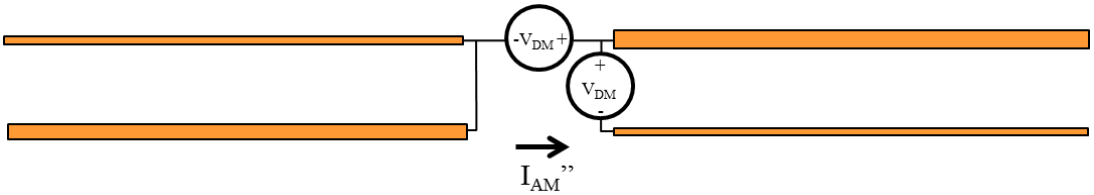

Fig. 16. Decomposition of the original circuit (2/2).

Other than the amplitude of the voltage sources, Fig. 15 and Fig. 16 are identical to the circuits in Fig. 8 and Fig. 11. As a result the AM currents, I_{AM}' and I_{AM}'', generated in Fig. 15 and Fig. 16 can be calculated as,

$$I_{AM}' = -V_{DM} / Z_{AM1-L} = -(V_{DM} / Z_{AM}) \cdot h_L,$$
$$I_{AM}'' = V_{DM} / Z_{AM1-R} = (V_{DM} / Z_{AM}) \cdot h_R. \quad (22)$$

The total AM current generated in the original circuit in Fig. 1 will be the sum of the AM currents in Fig. 15 and Fig. 16,

$$I_{AM} = I_{AM}' + I_{AM}'' = (V_{DM} / Z_{AM}) \cdot (h_R - h_L) \quad (23)$$

.

Combining (23) and (2) we get,

$$V_{AM} = V_{DM} \cdot (h_R - h_L) \ . \tag{24}$$

Equation (24) is the core equation of the IDT that has been used to model the DM-to-AM conversion in a wide variety of structures. Here, it is shown to be an exact relationship as long as the DM propagation is TEM and the imbalance factors are defined based on the antenna-mode current division as indicated in (4) and (5).

4. Calculation of Current Division Factor

4.1 Discussion of Previous Calculation Method

In published applications of IDT for radiated emission modeling [5]-[18], the current division factors are calculated using one of the following equations [5]:

$$h = \frac{C_{11}}{C_{11} + C_{22}} \ , \tag{25.a}$$

or

$$h = \frac{L_{22} - L_{12}}{L_{11} + L_{22} - 2L_{12}}. \tag{25.b}$$

These definitions of the current division factor (or imbalance factor) are not strictly equivalent to the current division factors in (4) and (5). In [6], (25.a) and (25.b) are derived assuming that the AM signals satisfy the telegrapher's equations (i.e. exhibit TEM propagation). In this case, C_{11}, C_{22}, L_{11}, L_{22}, and L_{12} are the per-unit-length parameters of a transmission line with a well-defined and nearby ground. For TEM propagation, the per-unit-length parameters can be determined using a 2D static field solver. For the static field solution, the ground can be moved farther and farther away from the conductors until its size and location no longer affect the solution. The per-unit-length parameters calculated with the ground essentially at infinity and (25.a) or (25.b) have been used to determine the imbalance factors by a number of researchers and have been successfully applied to modelling the radiated emissions of a wide variety of structures [6]-[19].

However, the AM currents are not TEM and do not satisfy the telegrapher's equations. It is reasonable to expect that the size and orientation of the conductor on one side of the antenna can have an effect on the current division factor on the other side. To illustrate this point, we drive a two-conductor TL with a quasi-static voltage source against another conductor, as shown in Fig. 17. The arrows in Fig. 17 represent the resulting electric field distribution. If the left side conductor is bent upwards, as indicated in Fig. 18, the field distribution near the two-conductor TL changes causing slightly more AM current to flow on the upper conductor of the TL. In other words, it is not possible to calculate the current division factor on one pair of conductors without accounting for the geometry of the entire 3D structure. Equations (25.a) and (25.b) which are based only on 2D, per-unit-length parameters cannot be precisely equal to (4) and (5) for arbitrary 3D geometries.

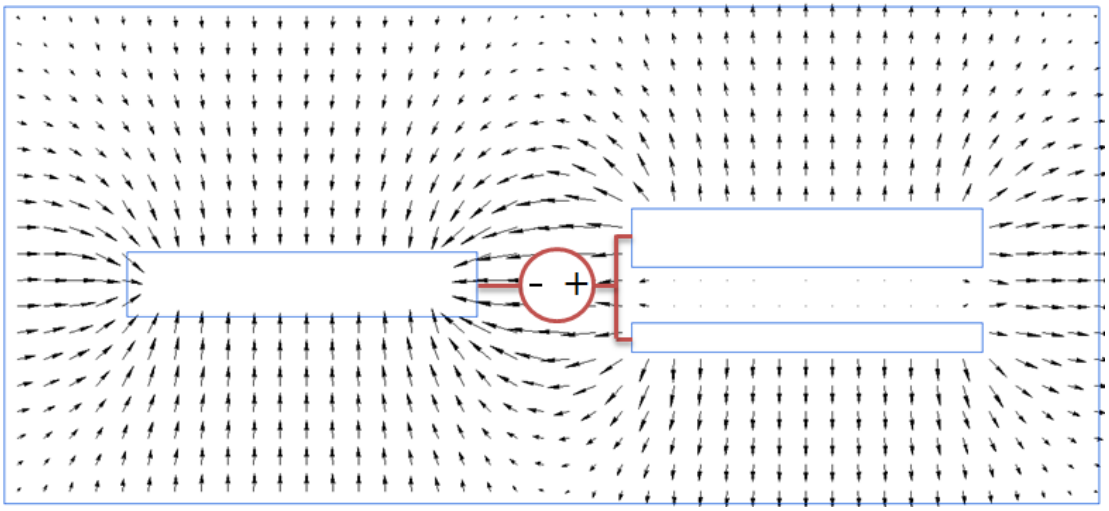

Fig. 17. Illustration of electric field distribution resulted from a quasi-static source driving a two-conductor transmission line relative to another wire.

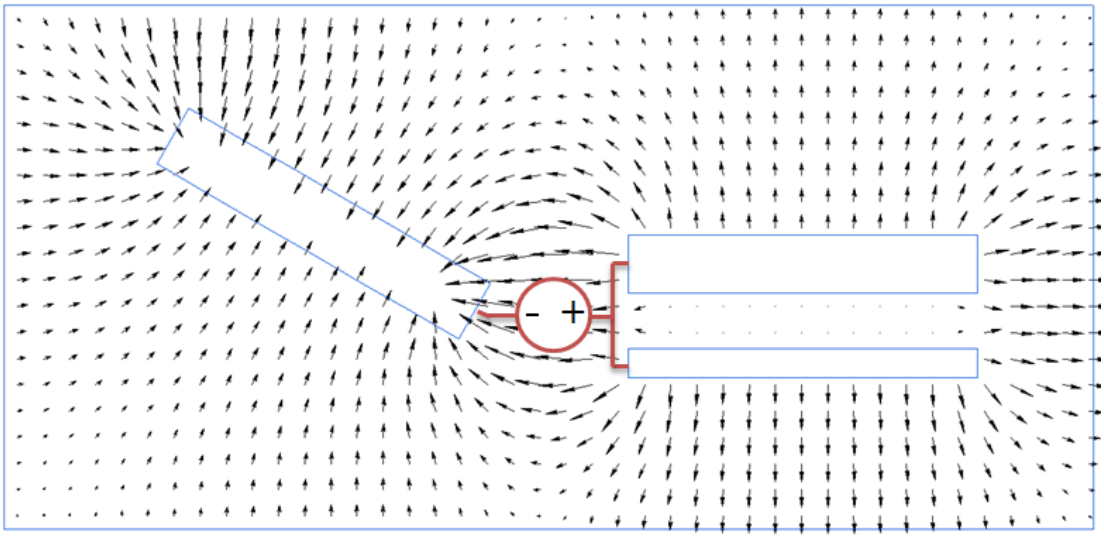

Fig. 18. Illustration of electric field distribution resulted from a quasi-static source driving a two-conductor transmission line relative to another angled wire.

However, even though the current division factor calculated using (25.a) or (25.b) is not mathematically exact, the following section will show that it is a very good approximation of the actual current division factor for most radiating structures of practical interest. This is because, for most monopole or dipole antenna structures, the geometry on one side of the antenna has very little effect on the field distribution near the conductor(s) on the other side.

4.2 Example Calculations

To examine how much the current division factor on one half of a dipole antenna is affected by the geometry of the other side, the current division factors of some example structures were calculated using a 3D full-wave field solver and compared to calculations made using a 2D static field solver. The 2D static field solver was QuickField Student Edition [20], which employs a finite element method. The 3D full-wave solver was FEKO [21], which is a method of moments code.

4.2.1 Description of the Example Structures

The first structure is shown in Fig. 19. A TL is formed by two wire conductors with circular cross-sections that have radii $R_1=1$ *mm* and $R_2=2$ *mm*. The wires are 12 mm apart. This TL is driven by an AM source relative to another wire conductor with radius $R_3=5$ *mm*. The lengths of all the wire conductors are 500 mm.

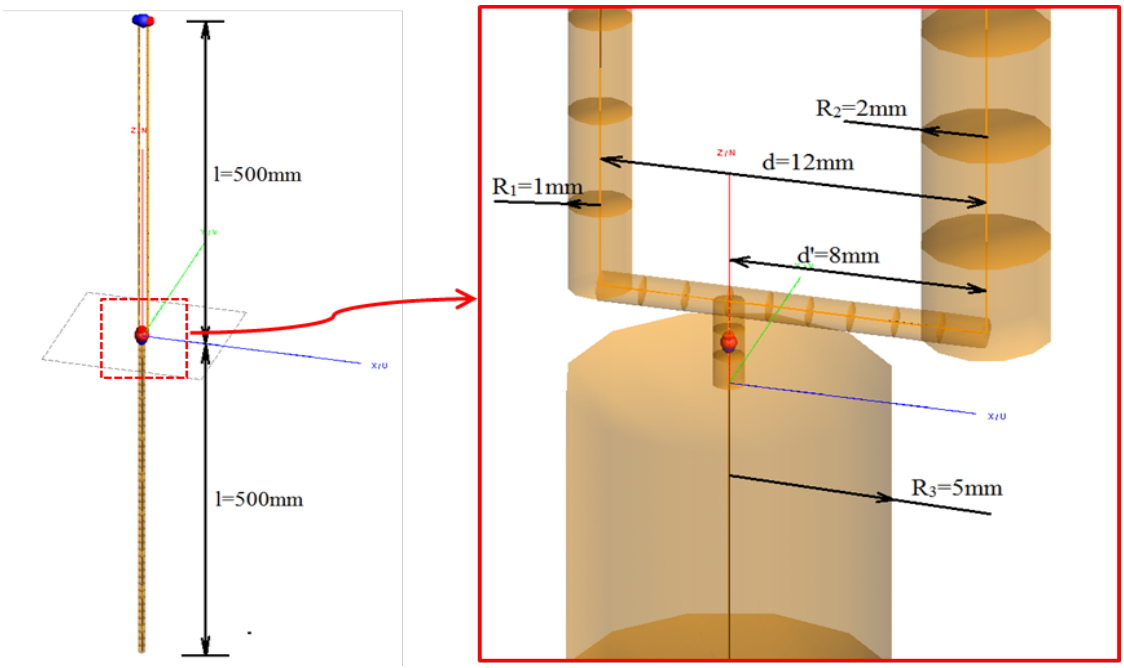

Fig. 19. Example Structure 1.

The second structure is shown in Fig. 20. The same TL as that in Structure 1 is driven by the same AM voltage source. On the other side of the AM source, instead of a wire, there is a metal sheet that is perpendicular to the TL. The metal sheet is connected to the AM source at the center of one edge and extends to the right side. This structure is intended to bias the current division factor by making it easier for current to flow on the right-side wire of the TL rather than the left-side wire.

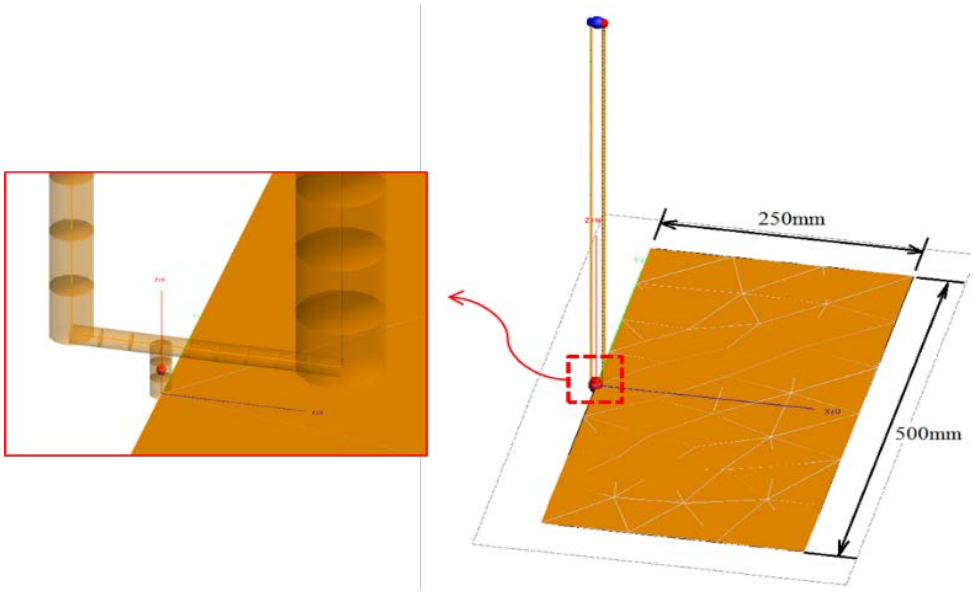

Fig. 20. Example Structure 2.

The third structure is similar to Structure 2 except that the metal sheet is flipped to the left side, so that it favors current flowing on the left-side wire of the TL, as shown in Fig. 21.

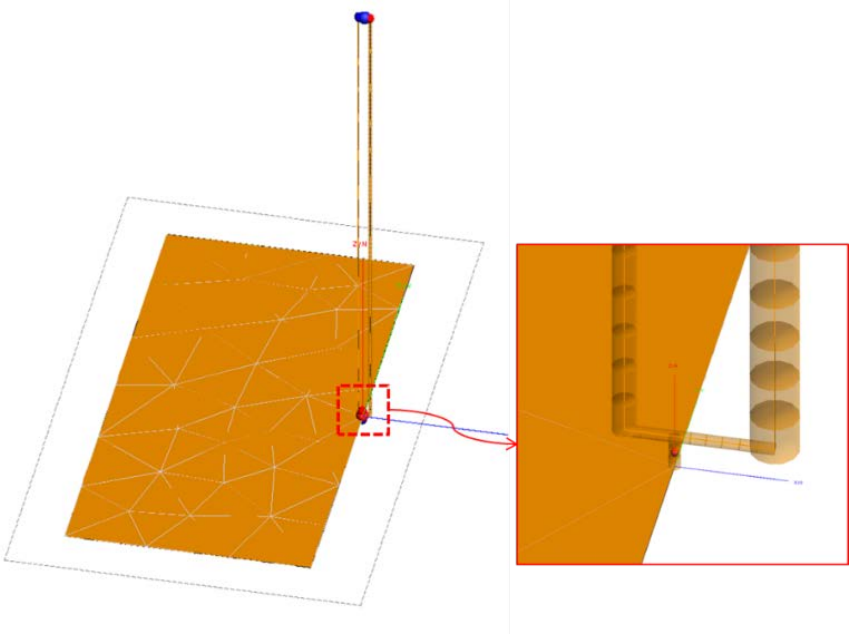

Fig. 21. Example Structure 3.

4.2.2 Calculation Results

Fig. 22 shows the calculated current division factors obtained using the 2D static field solver and 3D full-wave code over the frequency range from 30 MHz to 200 MHz.

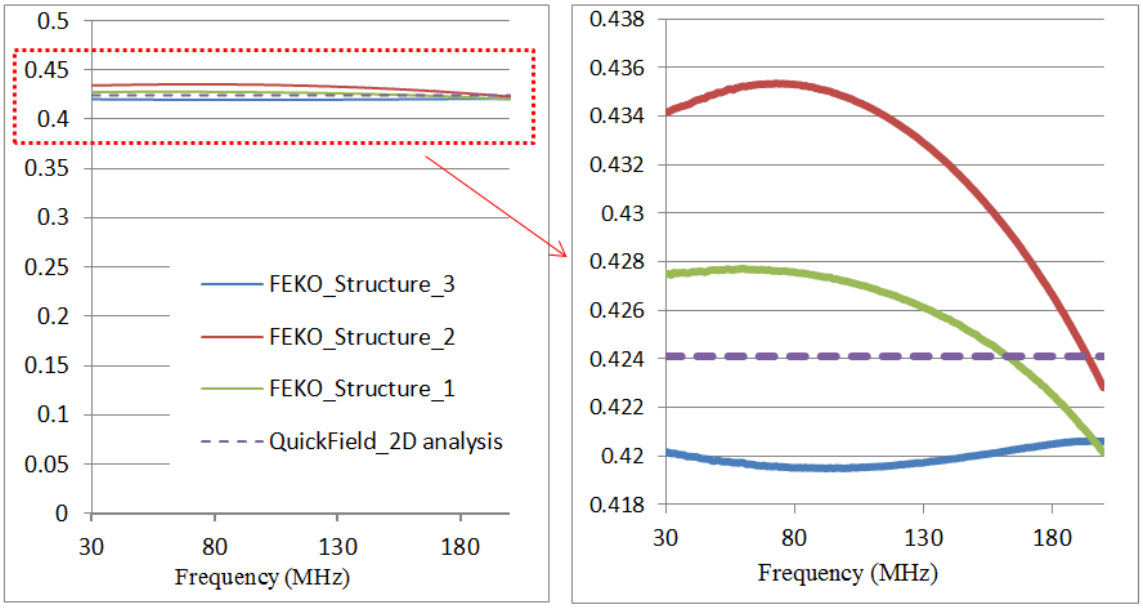

Fig. 22. Current division factor calculation result over 30MHz to 200MHz.

In Fig. 22, the three solid lines are current division factors calculated using FEKO, for Structures 1, 2, and 3. All of them are curved over frequency, which means the actual current division factor is a weak

function of frequency. The relative positions of these three solid lines are consistent with our expectation that the conductor on one wing of the antenna will affect the current distribution between two conductors on the other wing. However, for all three structures over the full frequency range, the biggest current division factor we obtained was 0.435 and the smallest was 0.419. The actual current division factor never deviated more than 2.6% from the 2D imbalance factor obtained using QuickField and (25.a). Since the asymmetry in these examples was greater than that which would be encountered in most practical situations, it can be concluded that the 2D per-unit-length calculations in (25) will generally provide a fairly accurate estimate of the current division factor.

5. Conclusion

The imbalance difference theory as applied to radiated emission modeling has been derived rigorously without making any assumptions related to TEM propagation of the antenna-mode signals. The relationship between differential-mode voltage and antenna-mode voltage at points where there is a change in electrical balance is precisely described by (24) as long as the differential-mode propagation is TEM and the current division factor, *h*, represents the actual division of antenna-mode current on the two transmission line conductors.

The second part of this paper demonstrates that the division of antenna-mode current on one half of a radiating dipole structure is relatively independent of the geometry of the other half. Therefore, (25.a) or (25.b), which rely on a simple 2D static-field analysis of the cross-section of the transmission line, provide an excellent approximation of the actual current division factor.

References

[1] C. R. Paul, “A comparison of the contributions of common-mode and differential-mode currents in radiated emissions,” *IEEE Trans. Electromagn. Compat.*, vol. 31, no. 2, pp. 189–193, May 1989.

[2] T. H. Hubing and J. F. Kaufman, “Modeling the electromagnetic radiation from electrically small table-top products,” *IEEE Trans. Electromagn. Compat.*, vol. 31, no. 1, pp. 74–84, 1989.

[3] K. Hardin and C. Paul, “Decomposition of radiating structures using the ideal structure extraction methods (ISEM),” *IEEE Trans. Electromagn. Compat.*, vol. 35, no. 2, pp. 264-273, May 1993.

[4] D. M. Hockanson, J. L. Drewniak, T. H. Hubing, T. P. Van Doren, F. Sha, and M. Wilhelm, "Investigation of fundamental EMI source mechanisms driving common mode radiation from printed circuit boards with attached cables," *IEEE Trans. Electromagn. Compat.*, vol. 38, no. 4, Nov. 1996, pp. 557-566.

[5] T. Watanabe, O. Wada, T. Miyashita, and R. Koga, “Common-Mode-Current Generation Caused by Difference of Unbalance of Transmission Lines on a Printed Circuit Board with Narrow Ground Pattern,” *IEICE Trans. Commun.*, vol. E83-B, no. 3, pp. 593–599, Mar. 2000.

[6] T. Watanabe, H. Fujihara, O. Wada, R. Koga, and Y. Kami, “A Prediction Method of Common-Mode Excitation on a Printed Circuit Board Having a Signal Trace near the Ground Edge,” *IEICE Trans. Commun.*, vol. E87-B, no. 8, pp. 2327–2334, Aug. 2004.

[7] T. Watanabe, O. Wada, Y. Toyota, and R. Koga, “Estimation of common-mode EMI caused by a signal line in the vicinity of ground edge on a PCB,” in *IEEE International Symposium on Electromagnetic Compatibility*, 2002, vol. 1, pp. 113–118.

[8] T. Watanabe, M. Kishimoto, S. Matsunaga, T. Tanimoto, R. Koga, O. Wada, and A. Namba, “Equivalence of two calculation methods for common-mode excitation on a printed circuit board with narrow ground plane,” in *2003 IEEE Symposium on Electromagnetic Compatibility. Symposium Record* (Cat. No.03CH37446), 2003, vol. 1, pp. 22–27.

[9] O. Wada, “Modeling and simulation of unintended electromagnetic emission from digital circuits,” *Electron. Commun*. Japan (Part I Commun., vol. 87, no. 8, pp. 38–46, Aug. 2004.

[10] Y. Toyota, A. Sadatoshi, T. Watanabe, K. Iokibe, R. Koga, and O. Wada, “Prediction of electromagnetic emissions from PCBs with interconnections through common-mode antenna model,” in *2007 18th International Zurich Symposium on Electromagnetic Compatibility*, 2007, pp. 107–110.

[11] Y. Toyota, T. Matsushima, K. Iokibe, R. Koga, and T. Watanabe, “Experimental validation of imbalance difference model to estimate common-mode excitation in PCBs,” in *2008 IEEE International Symposium on Electromagnetic Compatibility*, 2008, pp. 1–6.

[12] T. Matsushima, T. Watanabe, Y. Toyota, R. Koga, and O. Wada, “Evaluation of EMI Reduction Effect of Guard Traces Based on Imbalance Difference Model,” *IEICE Trans. Commun.*, vol. E92-B, no. 6, pp. 2193–2200, Jun. 2009.

[13] T. Matsushima, T. Watanabe, Y. Toyota, R. Koga, and O. Wada, “Increase of Common-Mode Radiation due to Guard Trace Voltage and Determination of Effective Via-Location,” *IEICE Trans. Commun.*, vol. E92-B, no. 6, pp. 1929–1936, Jun. 2009.

[14] C. Su and T. H. Hubing, “Imbalance Difference Model for Common-Mode Radiation from Printed Circuit Boards,” *IEEE Trans. Electromagn. Compat.*, vol. 53, no. 1, pp. 150–156, Feb. 2011.

[15] K. Sejima, Y. Toyota, K. Iokibe, L. R. Koga, and T. Watanabe, “Experimental model validation of mode-conversion sources introduced to modal equivalent circuit,” *2012 IEEE Int. Symp. Electromagn. Compat.*, pp. 492–497, Aug. 2012.

[16] T. Matsushima, O. Wada, T. Watanabe, Y. Toyota, and L. R. Koga, “Verification of common-mode-current prediction method based on imbalance difference model for single-channel differential signaling system,” in *2012 Asia-Pacific Symposium on Electromagnetic Compatibility*, 2012, vol. 2, pp. 409–412.

[17] A. Sugiura and Y. Kami, “Generation and Propagation of Common-Mode Currents in a Balanced Two-Conductor Line,” *IEEE Trans. Electromagn. Compat.*, vol. 54, no. 2, pp. 466–473, Apr. 2012.

[18] H. Al-Rubaye, K. Pararajasingam, and M. Kane, “Estimating radiated emissions from microstrip transmission lines based on the imbalance model,” in *2012 IEEE Electrical Design of Advanced Packaging and Systems Symposium (EDAPS)*, 2012, pp. 93–96.

[19] H. Kwak and T. H. Hubing, “Investigation of the imbalance difference model and its application to various circuit board and cable geometries,” in *2012 IEEE International Symposium on Electromagnetic Compatibility*, 2012, pp. 273–278.

[20] “QuickField Student Edition.” [Online]. Available: http://www.quickfield.com/free_soft.htm. [Accessed: 25-Jun-2014].

[21] FEKO User's Manual, Suite 6.2 2013.